Registry No. **1**, 129215-67-4; **2A**, 130611-13-1; **3**, 118575-30-7; **4**, 130574-84-4; **5**, 130574-88-8; **6A**, 130574-85-5; **6B**, 130694-29-0; **7**, 118575-35-2; **8**, 118575-32-9; **9**, 130574-86-6; **10A**, 130694-31-4; **10B**, 130694-32-5; **11A**, 130694-30-3; **11B**, 130790-16-8; $RuCl_2(PPh_3)_3$, 34076-51-2; $RuCl_2$(Cyttp), 84623-42-7; $RuH(P(OPh)_2OC_6H_4)$(Cyttp), 130574-87-7.

Supplementary Material Available: Tables (SUP-1-SUP-4 and SUP-6) of complete bond distances and angles, calculated positional parameters and *B* values for hydrogen atoms, anisotropic thermal parameters for the non-hydrogen atoms, and complete crystallographic data (7 pages); a table (SUP-5) of observed and calculated structure factors (17 pages). Ordering information is given on any current masthead page.

Contribution from the Department of Inorganic Chemistry, Indian Association for the Cultivation of Science, Calcutta 700032, India

Isomer Preference of Oxidation States. Chemistry of the $Os(xanthate)_2(PPh_3)_2^z$ ($z = 0, +$) Family

Amitava Pramanik, Nilkamal Bag, Debashis Ray, Goutam Kumar Lahiri, and Animesh Chakravorty*

Received May 7, 1990

The title family consist of cis isomers of osmium(II) ($z = 0$; **1**) and osmium(III) ($z = +$; $\mathbf{1}^+$) and the corresponding trans isomers (**2**, $\mathbf{2}^+$). Four xanthates, ROC(S)S$^-$ (Rx^-), have been used: R = Me, Et, *i*-Pr, $PhCH_2$. All complexes except $\mathbf{1}^+$ have been isolated in pure state in excellent yields: **1** by the reaction of $Os(PPh_3)_3Br_2$ with KRx, $\mathbf{2}^+$ via oxidation of **1** with cerium(IV), and **2** by the reduction of $\mathbf{2}^+$ by hydrazine hydrate. The formal potentials, $E°$(cis) and $E°$(trans), of the redox couples $\mathbf{1}^+$-**1** and $\mathbf{2}^+$-**2** are respectively ~0.4 and ~0.1 V vs SCE; the equilibrium constants K^{II} and K^{III} of the isomerization reactions $\mathbf{2} \rightleftharpoons \mathbf{1}$ and $\mathbf{1}^+ \rightleftharpoons \mathbf{2}^+$ are ~10 and ~10^4, respectively (CH_2Cl_2, 303 K). The metal oxidation states strongly differentiate the isomeric coordination spheres. The matched combinations are cis-Os^{II} (**1**) and trans-Os^{III} ($\mathbf{2}^+$). The mismatched species $\mathbf{1}^+$ and **2** are unstable and isomerize spontaneously in solution. To establish isomer structures and to probe the origin of the differentiation process, the X-ray structures of *cis*-$Os(Mex)_2(PPh_3)_2$ (**1a**), *trans*-$Os(Mex)_2(PPh_3)_2$ (**2a**), and *trans*-$[Os(Mex)_2(PPh_3)_2]PF_6 \cdot 2H_2O$ ($\mathbf{2a}^+$) have been determined. **1a**: space group *Pbca*, $Z = 8$, $a = 10.774$ (3) Å, $b = 18.580$ (7) Å, $c = 38.043$ (6) Å, and $V = 7616$ (4) Å^3. **2a**: space group $P\bar{1}$, $Z = 1$, $a = 9.231$ (4) Å, $b = 10.466$ (5) Å, $c = 11.149$ (5) Å, $\alpha = 101.33$ (3)°, $\beta = 108.66$ (3)°, $\gamma = 108.02$ (3)°, and $V = 916.8$ (7) Å^3. $\mathbf{2a}^+$: space group $P\bar{1}$, $Z = 1$, $a = 9.766$ (4) Å, $b = 11.363$ (5) Å, $c = 11.677$ (5) Å, $\alpha = 112.19$ (4)°, $\beta = 105.13$ (4)°, $\gamma = 97.17$ (4)°, and $V = 1121.6$ (9) Å^3. The binding in the OsS_4 fragment is primarily σ in nature. The mean Os-S distance *decreases* upon metal oxidation: **1a**, 2.424 (5) Å; **2a**, 2.410 (2) Å; $\mathbf{2a}^+$, 2.378 (2) Å. The OsP_2 fragment is subject to $5d\pi$-$3d\pi$ back-bonding, which decreases rapidly in the order $\mathbf{1a} > \mathbf{2a} > \mathbf{2a}^+$, leading to a large and progressive increase in mean Os-P length: **1a**, 2.317 (4) Å; **2a**, 2.365 (4) Å; $\mathbf{2a}^+$, 2.439 (3) Å. The stability order $\mathbf{1} > \mathbf{2}$ as well as the redox potential order $E°$(cis) > $E°$(trans) arises primarily from the superior Os-P back-bonding in **1** compared to **2**. Due to the poor back-bonding ability of osmium(III), steric factors become controlling and this explains the stability of $\mathbf{2}^+$ over $\mathbf{1}^+$. Paramagnetic ($S = {}^1/_2$) $\mathbf{2}^+$ affords strongly rhombic EPR spectra—the axial and rhombic distortion parameters being ~7000 and ~2000 cm^{-1}, respectively. A weak optical transition within the Kramers doublets is observable near 7600 cm^{-1}.

Introduction

This work stems from our interest in the differentiation of isomeric coordination spheres by unequal oxidation states of the same metal ion.[1-4] Herein we describe examples of this phenomenon in osmium(II,III) chemistry using a family of OsS_4P_2 complexes assembled from xanthates and triphenylphosphine. The synthesis and characterization of geometrical isomers are described. The preferred geometries are cis for osmium(II) and trans for osmium(III). Mismatched combinations of oxidation state and geometrical configuration can be imposed by rapid redox, but these relax via spontaneous isomerization. Such processes have been thermodynamically and kinetically quantitated by using voltammetric and spectroscopic techniques. The origin of isomer preference of oxidation states is probed by X-ray structure determination of three complexes differing in geometry and/or oxidation state. Osmium-phosphine back-bonding is shown to play a pivotal role.

Scheme I[a]

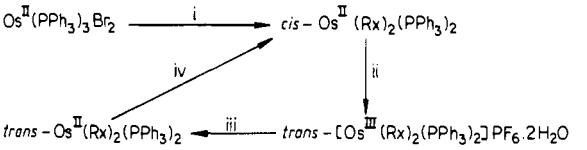

[a] Legend: (i) KRx, EtOH, boil; (ii) CH_2Cl_2-CH_3CN(1:10), $(NH_4)_4Ce(SO_4)_4 \cdot 2H_2O$-$H_2O$, stir, NH_4PF_6-H_2O; (iii) CH_3CN, $NH_2NH_2 \cdot H_2O$, stir under N_2 atm., 273K; (iv) CH_2Cl_2, warm.

Results

A. Complexes and Their Synthesis. The four subgroups of the $Os(Rx)_2(PPh_3)_2^z$ ($Rx^- = ROC(S)S^-$; $z = 0, +$) family correspond to cis-osmium(II) (**1**), cis-osmium(III) ($\mathbf{1}^+$), trans-osmium(II) (**2**), and trans-osmium(III) ($\mathbf{2}^+$). All but $\mathbf{1}^+$ have been isolated

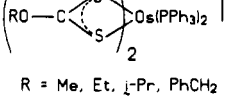

R = Me, Et, *i*-Pr, $PhCH_2$

1 cis, $z = 0$

$\mathbf{1}^+$ cis, $z = +$

2 trans, $z = 0$

$\mathbf{2}^+$ trans, $z = +$

(1) (a) Ray, D.; Chakrovorty, A. *Inorg. Chem.* **1988**, *27*, 3292-3297. (b) Basu, P.; Bhanja Choudhury, S.; Pal, S.; Chakravorty, A. *Inorg. Chem.* **1989**, *28*, 2680-2686. (c) Basu, P.; Pal, S.; Chakravorty, A. *J. Chem. Soc., Chem. Commun.* **1989**, 977-978. (d) Bag, N.; Lahiri, G. K.; Chakravorty, A. *J. Chem. Soc., Dalton Trans.* **1990**, 1557-1561.

(2) (a) Bond, A. M.; Grabaric, B. S.; Grabaric, Z. *Inorg. Chem.* **1978**, *17*, 1013-1018. (b) Bond, A. M.; Carr, S. W.; Colton, R. *Inorg. Chem.* **1984**, *23*, 2343-2350. (c) Bond, A. M.; Hambley, T. W.; Mann, D. R.; Snow, M. R. *Inorg. Chem.* **1987**, *26*, 2257-2265 and references therein.

(3) (a) Rieke, R. D.; Kojima, H.; Ofele, K. *J. Am. Chem. Soc.* **1976**, *98*, 6735-6737. (b) Elson, C. M. *Inorg. Chem.* **1976**, *15*, 469-470. (c) Vallat, A.; Person, M.; Roullier, L.; Laviron, E. *Inorg. Chem.* **1987**, *26*, 332-335. (d) Bernardo, M. M.; Robandt, P. V.; Schroeder, R. R.; Rorabacher, D. B. *J. Am. Chem. Soc.* **1989**, *111*, 1224-1231.

(4) (a) Bursten, B. E. *J. Am. Chem. Soc.* **1982**, *104*, 1299-1304. (b) Mingos, D. M. P. *J. Organomet. Chem.* **1979**, *179*, C29-C33.

0020-1669/91/1330-0410$02.50/0

Table I. Electronic Spectral Data for *cis*- and *trans*-Os(Rx)$_2$(PPh$_3$)$_2$ and *trans*-[Os(Rx)$_2$(PPh$_3$)$_2$]PF$_6$·2H$_2$O at 298 K

compd	isomer	UV–vis data:[a] λ_{max}, nm (ϵ, M^{-1} cm^{-1})	compd	UV–vis–near-IR data:[a] λ_{max}, nm (ϵ, M^{-1} cm^{-1})
Os(Mex)$_2$(PPh$_3$)$_2$	cis	450[b] (870), 360 (3850), 280 (9130)	*trans*-[Os(Mex)$_2$(PPh$_3$)$_2$]PF$_6$·2H$_2$O	1300 (32), 640 (3080), 470[b] (650), 370 (4420), 260 (28 980)
	trans	520 (1050), 390 (4680)		
Os(Etx)$_2$(PPh$_3$)$_2$	cis	450[b] (1000), 360 (4360), 280 (9640)	*trans*-[Os(Etx)$_2$(PPh$_3$)$_2$]PF$_6$·2H$_2$O	1300 (35), 640 (3320), 470[b] (770), 370 (5000), 270 (30 210)
	trans	520 (1150), 390 (4800)		
Os(i-Prx)$_2$(PPh$_3$)$_2$	cis	460[b] (700), 360 (3420), 290 (7550)	*trans*-[Os(*i*-Prx)$_2$(PPh$_3$)$_2$]PF$_6$·2H$_2$O	1300 (37), 650 (3400), 465[b] (780), 370 (5350), 270 (30 770)
	trans	520 (1120), 380 (5160)		
Os(PhCH$_2$x)$_2$(PPh$_3$)$_2$	cis	450[b] (1100), 370 (5200), 290 (11 500)	*trans*-[Os(PhCH$_2$x)$_2$(PPh$_3$)$_2$]PF$_6$·2H$_2$O	1250 (57), 640 (2980), 465[b] (1080), 360 (5450), 260 (28 190)
	trans	520 (1100), 390 (5200)		

[a] The solvent is dichloromethane. [b] Shoulder.

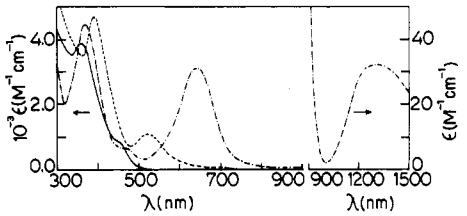

Figure 1. Electronic spectra of *cis*-Os(Mex)$_2$(PPh$_3$)$_2$ (—), *trans*-Os(Mex)$_2$(PPh$_3$)$_2$ (- - -), and *trans*-[Os(Mex)$_2$(PPh$_3$)$_2$]PF$_6$·2H$_2$O (···) in dichloromethane.

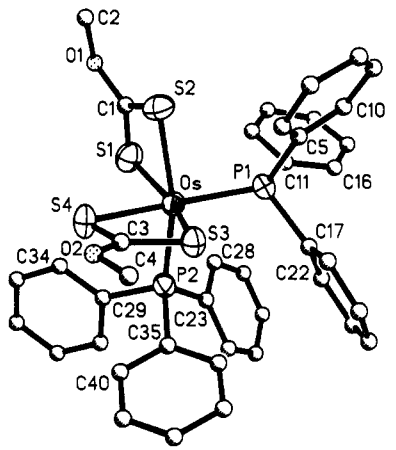

Figure 2. ORTEP plot and labeling scheme for *cis*-Os(Mex)$_2$(PPh$_3$)$_2$.

in the pure state (Table I). Ruthenium analogues of **1** are known,[1d,5] but none of the few osmium xanthates described in the literature[5a,6] belong to the present family.

The synthetic reactions are stated in Scheme I. The primary reaction involving Os(PPH$_3$)$_3$Br$_2$ and KRx is carried out in boiling ethanol, and the pure *cis*-Os(Rx)$_2$(PPh$_3$)$_2$ isomer deposits from the reaction mixture. Oxidation of *cis*-Os(Rx)$_2$(PPh$_3$)$_2$ in acetonitrile–dichloromethane mixture by aqueous cerium(IV) affords *trans*-Os(Rx)$_2$(PPh$_3$)$_2^+$ as the final product, which is isolated as the hexafluorophosphate dihydrate salt. The *cis*-Os(Rx)$_2$(PPh$_3$)$_2^+$ isomer is undoubtedly formed as the initial oxidation product only to isomerize rapidly enough to elude isolation. Synthesis of *trans*-Os(Rx)$_2$(PPh$_3$)$_2$ involves reduction of **2**$^+$ in acetonitrile solution by hydrazine hydrate at 273 K. This isomer is metastable, and if left in solution, it slowly (hence the success in its isolation) isomerizes to the cis congener.

The yield in each of the synthetic steps is excellent. The complexes have distinctive colors both in the solid state and in solution: **1**, yellow; **2**, red; **2**$^+$, bluish green. Spectral data are shown in Table I, and representative spectra are displayed in Figure 1. The **2**$^+$ complexes are 1:1 electrolytes in acetonitrile solution (Λ = 140–150 Ω^{-1} cm^2 M^{-1}) and are EPR-active one-electron paramagnets (see below).

Table II. Selected Bond Distances (Å) and Angles (deg) and Their Estimated Standard Deviations for *cis*-Os^{II}(Mex)$_2$(PPh$_3$)$_2$ (**1a**), *trans*-Os^{II}(Mex)$_2$(PPh$_3$)$_2$ (**2a**), and *trans*-[Os^{III}(Mex)$_2$(PPh$_3$)$_2$]PF$_6$·2H$_2$O (**2a**$^+$)

	1a	**2a**	**2a**$^+$
	Distances		
Os–P(1)	2.333 (4)	2.365 (2)	2.439 (3)
Os–P(2)	2.301 (4)		
Os–S(1)	2.396 (5)	2.411 (2)	2.378 (2)
Os–S(2)	2.457 (5)	2.409 (3)	2.377 (3)
Os–S(3)	2.393 (4)		
Os–S(4)	2.450 (5)		
	Angles		
P(1)–Os–S(1)	104.4 (2)	84.0 (1)	87.0 (1)
P(1)–Os–S(2)	91.1 (2)	91.9 (1)	94.9 (1)
S(2)–Os–S(1)	70.9 (2)	71.0 (1)	72.3 (1)
P(1)–Os–P(2)	100.8 (2)		
P(1)–Os–S(3)	92.1 (1)		
P(1)–Os–S(4)	161.8 (2)		
P(2)–Os–S(1)	95.2 (2)		
P(2)–Os–S(2)	163.7 (2)		
P(2)–Os–S(3)	94.5 (2)		
P(2)–Os–S(4)	87.8 (2)		
S(3)–Os–S(1)	158.8 (1)		
S(4)–Os–S(1)	90.6 (2)		
S(2)–Os–S(4)	84.0 (2)		
S(3)–Os–S(4)	71.0 (2)		
S(3)–Os–S(2)	96.1 (2)		

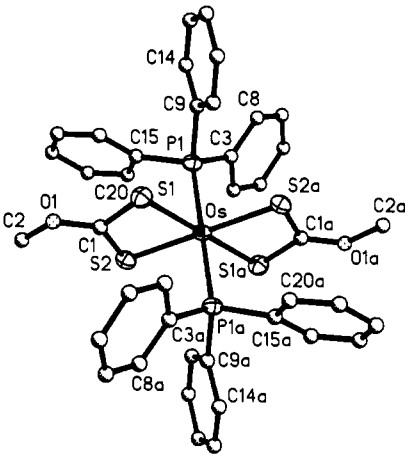

Figure 3. ORTEP plot and labeling scheme for *trans*-Os(Mex)$_2$(PPh$_3$)$_2$.

B. Crystal and Molecular Structures. One member (R = Me) of each type was chosen for structure determination: *cis*-Os(Mex)$_2$(PPh$_3$)$_2$ (**1a**), *trans*-Os(Mex)$_2$(PPh$_3$)$_2$ (**2a**), and *trans*-[Os(Mex)$_2$(PPh$_3$)$_2$]PF$_6$·2H$_2$O (**2a**$^+$). Views of the Os(Mex)$_2$-

(5) (a) Critchlow, P. B.; Robinson, S. D. *J. Chem. Soc., Dalton Trans.* **1975**, 1367–1372. (b) O'Connor, C.; Gilbert, J. D.; Wilkinson, G. *J. Chem. Soc. A* **1969**, 84–87.
(6) Cole-Hamilton, D. J.; Stephenson, T. A. *J. Chem. Soc., Dalton Trans.* **1976**, 2396–2405.

Table III. Bulk Magnetic Moments,[a] EPR g Values,[b,c] Distortion Parameters, and Near-IR Transitions

compd	μ_{eff}, μ_B	g_x	g_y	g_z	Δ/λ	V/λ	ν_1/λ	ν_2/λ	$(\nu_1/\lambda)_{obsd}$[d]
trans-$[Os(Mex)_2(PPh_3)_2]PF_6 \cdot 2H_2O$	1.90	2.836	2.535	1.400	2.457	−0.752	2.279	3.334	2.560
trans-$[Os(Etx)_2(PPh_3)_2]PF_6 \cdot 2H_2O$	1.87	2.882	2.546	1.394	2.466	−0.824	2.264	3.368	2.560
trans-$[Os(i\text{-}Prx)_2(PPh_3)_2]PF_6 \cdot 2H_2O$	1.78	2.877	2.494	1.363	2.398	−0.916	2.179	3.341	2.560
trans-$[Os(PhCH_2x)_2(PPh_3)_2]PF_6 \cdot 2H_2O$	1.85	2.809	2.519	1.404	2.453	−0.734	2.281	3.324	2.670

[a] In the solid state at 298 K. [b] In 1:1 dichloromethane–toluene frozen glass (77 K). [c] Signs of g values are negative, negative, and positive for g_x, g_y, and g_z, respectively. [d] Observed frequency converted to ν_1/λ by setting $\lambda = 3000$ cm^{-1}.

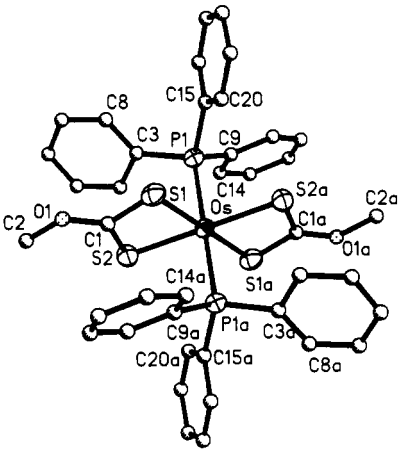

Figure 4. ORTEP plot and labeling scheme for the cation of *trans*-$[Os(Mex)_2(PPh_3)_2]PF_6 \cdot 2H_2O$.

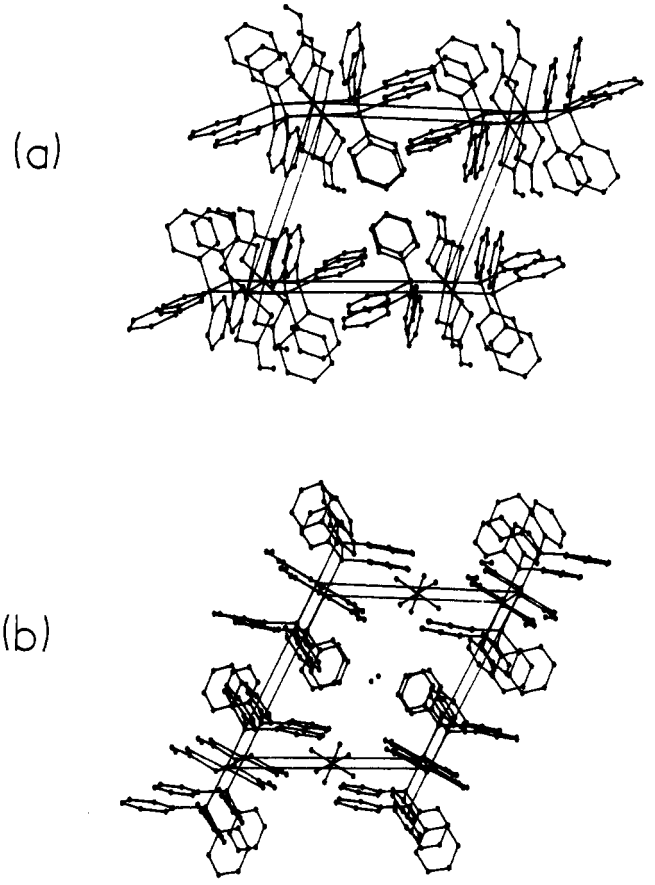

Figure 5. Cell packing diagrams of (a) *trans*-$Os(Mex_2(PPh_3)_2$ and (b) *trans*-$[Os(Mex)_2(PPh_3)_2]PF_6 \cdot 2H_2O$, viewed down the a axis.

$(PPh_3)_2$ moieties and atom-numbering schemes are shown in Figures 2–4. Selected bond parameters are listed in Table II.

The crystallographic similarity of the two trans complexes is noteworthy. They belong to the same space group ($P\bar{1}$), and in both cases the metal atom occupies a special position (0, 0, 0) imposing molecular centrosymmetry. Molecular packing is

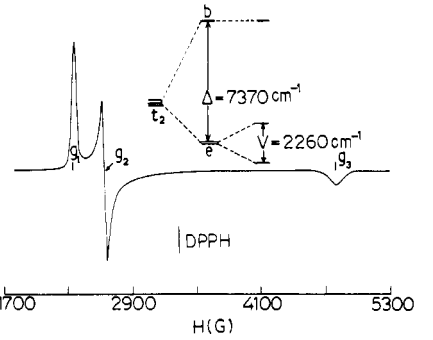

Figure 6. X-Band EPR spectrum and t_2 splittings of *trans*-$[Os(Mex)_2(PPh_3)_2]PF_6 \cdot 2H_2O$ in 1:1 dichloromethane–toluene glass (77 K).

dominated by phenyl rings. In going from the bivalent to the trivalent complex, molecules realign in the lattice and the cell dilates to accommodate the centrosymmetric hexafluorophosphate (phosphorus at $^1/_2$, 0, $^1/_2$) as well as water molecules of crystallization (Figure 5).

The chelate rings are excellent planes in all the three complexes. Due to the very acute chelate bite angle as well as due to steric hindrance of cis phosphine ligands, the OsS_4P_2 coordination sphere in **1a** is severely distorted (C_1 point group) from idealized octahedral geometry. Thus, the P(1)–Os–P(2) angle is 100.8 (2)° and all the three D–Os–D′ angles lie near 160° (D and D′ are donor atoms trans to one another). In **2a** and $\mathbf{2a}^+$ the D–Os–D′ angles are exactly 180° due to inversion symmetry. Here chelate bite is the main source of angular deviation from octahedral geometry—the angles between interchelate donor atoms in cis positions being as large as 109.0 (1)° (S(1)–Os–S(2a) in **2a**). The POsP axis is not quite perpendicular to the plane of the chelate rings but is slightly tilted toward S(1) in both the trans complexes. The point group symmetry of the coordination sphere in both the cases approaches C_{2h} but is strictly C_i only.

The low symmetry of **1a** is reflected in the unequal Os–P distances: 2.301 (4), 2.333 (4) Å. These values are significantly shorter than 2.365 (2) Å, which is the Os–P distance in **2a**. The distance increases to 2.439 (3) Å in $\mathbf{2a}^+$. In **1a** the Os–S distances fall into two distinct groups. The larger distances averaging 2.453 (5) Å correspond to sulfur atoms trans to phosphorus atom, and the shorter distances averaging 2.394 (4) Å are for the other S atoms. In **2a** and Os–S distance is 2.410 (2) Å and this decreases to 2.378 (2) Å in $\mathbf{2a}^+$. In summary, mean Os–P distances vary as $\mathbf{1} < \mathbf{2a} \ll \mathbf{2a}^+$, while mean Os–S distances follow the order $\mathbf{1a} \sim \mathbf{2a} > \mathbf{2a}^+$. The distances (C–O, C–S) within the Rx^- ligand do not show any significant variations among the three complexes, and the values agree with those in other xanthate complexes.[7]

C. EPR Spectra of Trans Osmium(III) Complexes. The magnetic moment of *trans*-$[Os(Rx)_2(PPh_3)_2]PF_6 \cdot 2H_2O$ corresponds to one unpaired electron (Table III). The EPR spectra

(7) (a) Chen, H. W.; Fackler, J. P., Jr. *Inorg. Chem.* **1978**, *17*, 22–26. (b) Hoskins, B. F.; Tiekink, E. R. T.; Winter, G. *Z. Kristallogr.* **1985**, *172*, 257–261. (c) Gable, R. W.; Hoskins, B. F.; Winter, G. *Inorg. Chim. Acta* **1985**, *96*, 151–159. (d) Bizilz, K.; Hardin, S. G.; Hoskins, B. F.; Oliver, P. J.; Tiekink, E. R. T.; Winter, G. *Aust. J. Chem.* **1986**, *39*, 1035–1042. (e) Edwards, A. J.; Hoskins, B. F.; Winter, G. *Aust. J. Chem.* **1986**, *39*, 1983–1991. (f) Tiekink, E. R. T.; Winter, G. *Aust. J. Chem.* **1986**, *39*, 813–816. (g) Tiekink, E. R. T. *Z. Kristallogr.* **1987**, *181*, 251–255. (h) Snow, M. R.; Tiekink, E. R. T. *Aust. J. Chem.* **1987**, *40*, 743–750. (i) Choudhury, S.; Ray, D.; Chakravorty, A. *Inorg. Chem.* **1990**, *29*, 4603.

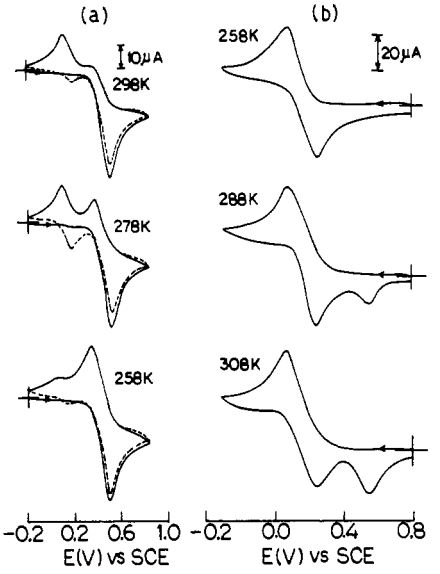

Figure 7. Variable-temperature cyclic voltammograms (scan rate 50 mV s^{-1}) of ~10^{-3} M solutions (a) *cis*-Os(Mex)$_2$(PPh$_3$)$_2$ (first cycle (—) and second cycle (---)) and (b) *trans*-[Os(Mex)$_2$(PPh$_3$)$_2$]PF$_6$·2H$_2$O in dichloromethane (0.1 M TEAP) at a platinum electrode.

of the complexes were examined (dichloromethane–toluene frozen glass, 77 K) for defining the nature and extent of deviation of osmium electronic structure from the octahedral standard. As expected from the crystallographic results, the spectra are rhombic in nature (Figure 6). These were analyzed with the help of **g**-tensor theory of d^5 ions, affording values of axial distortion (Δ), which split the t_2 shell into e + b and, the superimposed rhombic distortion (V), which splits e further into two nondegenerate components.[8,9] A pair of optical transitions (ν_1 and ν_2) among the three Kramers doublets are predicted (Table III) to lie at ~6700 and ~10000 cm^{-1} (the spin–orbit coupling constant λ of osmium(III) is taken as 3000 cm^{-1} [10]). A weak transition (ϵ ~ 40) is indeed observed at ~7600 cm^{-1} (Table I, Figure 1), and this is signed to ν_1. Due to the rapid rise in absorption pertaining to nearby intense transitions, the ν_2 band is not observable.

D. Electrochemistry. Voltammetric methods neatly reveal the interrelationship of metal redox and isomerization. Experiments were done in the temperature range 258–308 K in dichloromethane solution at a platinum electrode with a saturated calomel electrode (SCE) reference. Representative voltammograms for the R = Me complexes are shown in Figure 7.

At 298 K the one-electron (confirmed coulometrically) anodic peak of *cis*-Os(Rx)$_2$(PPh$_3$)$_2$ (**1**) (Figure 7a) is due to the stereoretentive oxidation to **1**$^+$. Rapid isomerization of electrogenerated **1**$^+$ to the trans isomer **2**$^+$ then occurs. Upon scan reversal the cathodic response due to process **1**$^+$ → **1** is therefore ill-defined but that due to **2**$^+$ → **2** is conspicuous. In second and subsequent cycles the anodic process **2** → **2**$^+$ for the trans complex also becomes observable. At lower temperatures the isomerization of **1**$^+$ to **2**$^+$ slows down with concomitant growth of the cathodic response of the cis isomer. Thus, the existence of the oxidized cis complex **1**$^+$ is electrochemically demonstrable although we have not succeeded in isolating it due to facile isomerization.

The low-temperature voltammogram of the trivalent *trans*-Os(Rx)$_2$(PPh$_3$)$_2^+$ (**2**$^+$) (Figure 7b) corresponds to an uncomplicated one-electron process involving **2**$^+$ and **2**. Isomerization of

Scheme II

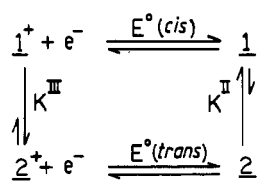

Table IV. Cyclic Voltammetric Formal Potentials of Isomers in Dichloromethane (0.1 M TEAP) at a Platinum Electrode at 298 K[a,b]

	osmium(III)–osmium(II)	
compd	$E°_{cis}$, V	$E°_{trans}$, V
Os(Mex)$_2$(PPh$_3$)$_2$	0.44	0.13
Os(EtX)$_2$(PPh$_3$)$_2$	0.42	0.11
Os(*i*-Prx)$_2$(PPh$_3$)$_2$	0.45	0.14
Os(PhCH$_2$x)$_2$(PPh$_3$)$_2$	0.47	0.16

[a] Scan rate 50 mV s^{-1}. [b] $E°$ is equal to the average of anodic (E_{pa}) and cathodic (E_{pc}) peak potentials.

Table V. Equilibrium Constants in Dichloromethane at 303 K

compd	K^{II} [a]	$10^{-3}K^{III}$ [b]
Os(Mex)$_2$(PPh$_3$)$_2$	12.44	11.50
Os(Etx)$_2$(PPh$_3$)$_2$	8.23	17.40
Os(*i*-Prx)$_2$(PPh$_3$)$_2$	6.30	22.70
Os(PhCH$_2$x)$_2$(PPh$_3$)$_2$	6.40	22.30

[a] Determined spectrophotometrically. [b] Listed values are derived from eq 4 with the help of K^{II} and K^{cr} (=1.43 × 10^5).

electrogenerated **2** becomes faster at higher temperatures, and the anodic peak of the cis isomer then becomes observable. At a given temperature the cyclic voltammetric behaviors of **2** (initial scan anodic) and **2**$^+$ (initial scan cathodic) are very similar as expected.

Bulk isomer synthesis and interconversion can be achieved coulometrically at constant potential. Thus, upon oxidation of **1** at 0.9 V one electron is transferred, rapid isomerization occurs, and the solution contains **2**$^+$ even when coulometry is done at 258 K. On the other hand when **2**$^+$ is coulometrically reduced at −0.2 V, the solution is found to contain only the metastable isomer **2**. If the reduced solution is left at 298 K, **2** isomerizes to **1** relatively slowly.

The observed voltammetric behavior of the complexes can thus be rationalized in terms of the isomerization and redox cycle of Scheme II. The values of $E°$(cis) and $E°$(trans), the formal potentials of the couples **1**$^+$–**1** and **2**$^+$–**2**, respectively, are listed in Table IV. The cis potentials (~0.4 V) are systematically ~300 mV more positive than the trans potentials (~0.1 V).

E. Isomerization Equilibria and Rates. The relevant equilibrium constants are K^{II} and K^{III} as defined in eqs 1 and 2 for the reactions

$$K^{II} = [\mathbf{1}]/[\mathbf{2}] \quad (1)$$

$$K^{III} = [\mathbf{2}^+]/[\mathbf{1}^+] \quad (2)$$

2 ⇌ **1** and **1**$^+$ ⇌ **2**$^+$, respectively. The constant K^{II} was directly determined (303 K) by monitoring the residual intensity of the 520-nm spectral band in equilibrated (10 h) solutions of **2**. This band is characteristic of **2** but is absent in **1** (Figure 1). At equilibrium more than 80% of the complex is in cis form. The constant K^{III} was estimated with the help of the cross-reaction of eq 3. The equilibrium constant of this reaction (eq 4) is derived

$$\mathbf{2} + \mathbf{1}^+ \overset{K^{cr}}{\rightleftharpoons} \mathbf{1} + \mathbf{2}^+ \quad (3)$$

$$K^{cr} = K^{II}K^{III} = \exp\left[\frac{F}{RT}(E°_T(\text{cis}) - E°_T(\text{trans}))\right] \quad (4)$$

with the help of the cycle of Scheme II. The value of K^{cr} is more or less constant at 1.43 × 10^5 for the present group of complexes. Values of K^{II} and K^{III} are listed in Table V. Thermodynamically the trivalent metal prefers the trans configuration and the bivalent metal the cis configuration. The former preference is much

(8) (a) Lahiri, G. K.; Bhattacharya, S.; Ghosh, B. K.; Chakravorty, A. *Inorg. Chem.* **1987**, *26*, 4324–4331. (b) Lahiri, G. K.; Bhattacharya, S.; Mukherjee, M.; Mukherjee, A. K.; Chakravorty, A. *Inorg. Chem.* **1987**, *26*, 3359–3365.
(9) (a) Bleaney, B.; O'Brien, M. C. M. *Proc. Phys. Soc. London, Sect. B* **1956**, *69*, 1216–1230. (b) Griffith, J. S. *The Theory of Transition Metal Ions*; Cambridge University Press: London, 1961; p 364.
(10) (a) Sakaki, S.; Hagiwara, N.; Yanase, Y.; Ohyoshi, A. *J. Phys. Chem.* **1978**, *82*, 1917–1920. (b) Hudson, A.; Kennedy, M. J. *J. Chem. Soc. A* **1969**, 1116–1120.

Table VI. Rate Constants and Activation Parameters in Dichloromethane

	trans → cis				cis$^+$ → trans$^+$			
compd	temp, K	10^5k^{II},[a] s^{-1}	ΔH^*, kcal/mol	ΔS^*, eu	temp, K	10^2k^{III},[b] s^{-1}	ΔH^*, kcal/mol	ΔS^*, eu
$Os(Mex)_2(PPh_3)_2$	303	8.20	22.02	−5.21	268	7.00	11.70	−20.50
	308	13.00			273	9.80		
	313	27.00			278	15.80		
$Os(Etx)_2(PPh_3)_2$	303	5.70	21.93	−6.07	268	5.20	13.25	−15.08
	308	10.60			273	9.40		
	313	18.50			278	13.10		

[a] Determined spectrophotometrically. [b] Determined cyclic voltammetrically.

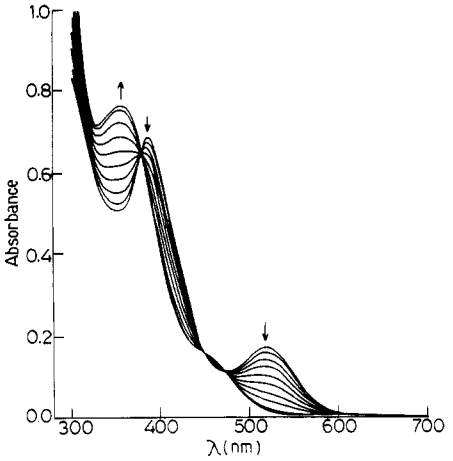

Figure 8. Electronic spectra of isomerizing solution of *trans*-$Os(Mex)_2(PPh_3)_2$ in dichloromethane at 303 K. The arrows indicate the increase and decrease of band intensities as the reaction proceeds.

stronger than the latter: $K^{III} \gg K^{II}$.

The isomerization reaction **2** → **1** can be followed spectrophotometrically (Figure 8). The reaction is first order with respect to **2**. Variable-temperature rate constants (k^{II}) and activation parameters for two systems are listed in Table VI. The rate constant (k^{III}) and activation parameters (Table VI) for the isomerization $\mathbf{1}^+ \rightarrow \mathbf{2}^+$ were determined cyclic voltammetrically[11] by using solutions of **1**. It is likely that the isomerization proceeds by a twist mechanism. Unfortunately, activation parameters are not good discriminators of alternative pathways.[12]

Discussion

The structural results reveal the gross features of the origin of isomer differentiation by the two oxidation states of osmium in $Os(Rx)_2(PPh_3)_2^z$. We consider the case of the bivalent state first. The mean Os–S distance in *cis*-$Os(Mex)_2(PPh_3)_2$ is equal to that in the trans congener to within 0.01 Å. The intraligand distances also do not show any major variations between the isomers. The mean Os–P distance is however 0.05 Å shorter in the cis isomer evidently due to stronger $5d\pi$–$3d\pi$ Os–P back-bonding. In this isomer all the three osmium $5d\pi$ orbitals are suited for π bonding, but this is not so in the trans isomer. The observed thermodynamic advantage of the cis-osmium(II) isomer is thus due to the stronger net chemical binding, which in turn originates primarily from superior back-bonding. Back-bonding stabilizes the metal $5d\pi$ orbitals, which therefore lie lower in the cis isomer. This is entirely consistent with the reduction potential trend $E°(\text{cis}) > E°(\text{trans})$, since the redox electron is a $5d\pi$ electron in both couples, $\mathbf{1}^+$–**1** and $\mathbf{2}^+$–**2**.

Back-bonding has a synergistic effect on σ interaction. The selective lengthening (trans effect) of Os–S bonds trans to Os–P bonds is thus understandable. It is being implied that the Os–S bonds are primarily σ in character. This is supported by the near independence of the Os–S bond length on isomeric structures as noted earlier as well as by the *decrease* of the length on metal oxidation.

This brings us to the trivalent state. The above-mentioned decrease in Os–S length amounts to ~0.03 Å between *trans*-$Os(Mex)_2(PPh_3)_2$ and *trans*-$Os(Mex)_2(PPh_3)_2^+$. The Os–P distance however *increases* by as much as ~0.07 Å, signifying *a large decrease in back-bonding upon metal oxidation.* To our knowledge, no other example of structural demonstration of this phenomenon in osmium chemistry exists at present. In the case of ruthenium instances of back-bonding-dependent bond length order Ru^{III}–N > Ru^{II}–N have been documented among complexes of π-accepting amines.[13] Back-bonding need not be totally absent[14] in *trans*-$Os(Mex)_2(PPh_3)_2^+$ but it must be quite weak, and the same is believed to be true for the elusive cis congener. In the case of osmium(III), isomer differentiation is therefore likely to be dictated by factors other than back-bonding. The PPh_3–PPh_3 steric interaction can be an important factor.[15] In a $(PPh_3)_2$ complex this would strongly favor the trans geometry.

The steric disadvantage of the cis configuration is clearly present in the osmium(II) species, and the structural data are supportive of this. Thus, the three carbon atoms directly bonded to P(1) are staggered (when viewed along the PP axis) with respect to those similarly bonded to P(2). The P(1)–Os–P(2) angle is accordingly obtuse to a good degree (100.8 (2)°).[15c] However, the electronic back-bonding factor more than offsets the steric disadvantage. The interplay of the two opposing factors can account for the substantial equilibrium concentration of the trans isomer in solutions of $Os(Rx)_2(PPh_3)_2$ ($K^{II} \sim 10$; Table V). On the other hand, in $Os(Rx)_2(PPh_3)_2^+$ the back-bonding factor is at best quite weak and equilibrium solutions contain mostly trans isomer in agreement with nearly total steric control ($K^{III} \sim 10^4$).

Last, we note that the known ruthenium(II) species of type $Ru(Rx)_2(PPh_3)_2$ are believed to have cis geometry.[5] A cycle of metal redox and geometrical isomerization supposedly similar to that of Scheme II has been realized but with only partial quantitation of equilibrium constants and rates.[1d] Single crystals could not however be grown, vitiating definitive characterization of isomers and the origin of isomerization.

Concluding Remarks

It has been demonstrated that the new family of osmium complexes, $Os(Rx)_2(PPh_3)_2^z$, constitute an observable redox–isomerization cycle membered by cis and trans forms of the $Os^{II}S_4P_2$ and $Os^{III}S_4P_2$ coordination spheres. The Os–S bonds are primarily σ in character, but Os–P bonds are involved in π back-bonding, which rapidly diminishes in the order cis-Os^{II} > trans-Os^{II} > trans-Os^{III}. The Os–P distance increases by a remarkable 0.12 Å between cis-Os^{II} and trans-Os^{III} (R = Me). The thermodynamic differentiation of cis and trans configurations by metal oxidation states as expressed in isomerization and redox equilibria has been rationalized on the basis of back-bonding and steric factors. Isomerization occurs either to maximize back-

(11) Nicholson, R. S.; Shain, I. *Anal. Chem.* **1964**, *36*, 706–723.
(12) Serpone, N.; Bickley, D. G. *Prog. Inorg. Chem.* **1972**, *17*, 391–566 and references therein.
(13) (a) Richardson, D. E.; Walker, D. D.; Sutton, J. E.; Hodgson, K. O.; Taube, H. *Inorg. Chem.* **1979**, *18*, 2216–2221. (b) Gress, M. E.; Creutz, C.; Quicksall, C. O. *Inorg. Chem.* **1981**, *20*, 1522–1528. (c) Eggleston, D. S.; Goldsby, K. A.; Hodgson, D. J.; Meyer, T. J. *Inorg. Chem.* **1985**, *24*, 4573–4580. (d) Wishart, J. F.; Bino, A.; Taube, H. *Inorg. Chem.* **1986**, *25*, 3318–3321.
(14) (a) Taube, H. *Pure Appl. Chem.* **1979**, *51*, 901–912. (b) Sekine, M.; Harman, W. D.; Taube, H. *Inorg. Chem.* **1988**, *27*, 3604–3608.
(15) (a) Tolman, C. A. *Chem. Rev.* **1977**, *77*, 313–348. (b) Clark, H. C.; Hampden-Smith, M. J. *Coord. Chem. Rev.* **1987**, *79*, 229–255. (c) Powell, J. *J. Chem. Soc., Chem. Commun.* **1989**, 200–202.

bonding where it matters most (Os^{II}: trans → cis) or to relieve steric crowding where back-bonding is weak (Os^{III}: cis → trans). Redox-induced isomerization promoted by back-bonding can take forms other than geometrical, e.g., the linkage isomerization of coordinated acetone between η^1- and η^2-bonding modes in pentaammineosmium chemistry.[16] Such rearrangements essentially originate in the domain involved in back-bonding and may (as in geometrical isomerization) or may not (as in linkage isomerization) require parallel reorganization in other domains of the coordination sphere.

Experimental Section

Materials. Osmium tetroxide obtained from Arora-Matthey, Calcutta, India was reacted with HX to afford $(NH_4)_2OsX_6$ (X = Cl, Br).[17] The compound $Os(PPh_3)_3Br_2$ was prepared according to the reported procedure.[18] Preparation of potassium xanthates (KRx) and purification of alcohols followed reported routes.[19] Electrochemically pure dichloromethane, acetonitrile, and tetraethylammonium perchlorate (TEAP) were obtained as before.[20] All other chemicals and solvents were of reagent grade and used without further purification.

Physical Measurements. Electronic spectra were recorded with a Hitachi 330 spectrophotometer fitted with a thermostated cell compartment. Infrared spectra (4000–300 cm^{-1}) were taken on a Perkin-Elmer 783 spectrophotometer. X-band EPR spectra were recorded on a Varian E-109C spectrometer fitted with a quartz Dewar flask for measurements at 77 K (liquid nitrogen). The spectra were calibrated with respect to DPPH (g = 2.0037). Electrochemical measurements were done by using a PAR Model 370-4 electrochemistry system incorporating the following: Model 174A polarographic analyzer; Model 175 universal programmer; Model RE0074 XY recorder; Model 173 potentiostat; Model 179 digital coulometer; Model 377 cell system. A planar Beckman Model 39273 platinum-inlay working electrode, a platinum-wire auxiliary electrode, and an aqueous saturated calomel reference electrode (SCE) were used in three-electrode measurements. A platinum-wire-gauze working electrode was used in coulometric experiments. All experiments were performed under dinitrogen atmosphere and reported potentials are uncorrected for junction contribution. Haake Model-F3K and Model-D8G digital cryostats and circulators connected to appropriate jacketed cells were used for low-temperature measurements. Magnetic susceptibilities were measured on a PAR-155 vibrating-sample magnetometer fitted with a Walker Scientific magnet. Solution electrical conductivity was measured by using a Philips PR 9500 bridge. Microanalyses (C, H, N) were done by using a Perkin-Elmer 240C elemental analyzer.

Preparation of Compounds. The syntheses of complexes were achieved by using general procedures. Yields varied in the range 85–95%. Details are given only for one representative complex of each type.

***cis*-Bis(methylxanthato)bis(triphenylphosphine)osmium(II), *cis*-Os(Mex)$_2$(PPh$_3$)$_2$.** $Os(PPh_3)_3Br_2$ (200 mg, 0.18 mmol) was suspended in 35 mL of ethanol. This mixture was warmed, and to this was added KMex (60 mg, 0.41 mmol). The mixture was heated to reflux for $^1/_2$ h and then cooled. An orange-yellow microcrystalline solid separated, which was collected by filtration, washed thoroughly with water and ethanol, and finally dried in vacuo over P_4O_{10}.

Anal. Calcd for Os(Mex)$_2$(PPh$_3$)$_2$, $OsC_{40}H_{36}O_2S_4P_2$: C, 51.71; H, 3.88. Found: C, 51.52, H, 3.97. Calcd for Os(Etx)$_2$(PPh$_3$)$_2$, $OsC_{42}H_{40}O_2S_4P_2$: C, 52.71; H, 4.18. Found: C, 52.49; H, 4.01. Calcd for Os(*i*-Prx)$_2$(PPh$_3$)$_2$, $OsC_{44}H_{44}O_2S_4P_2$: C, 53.65; H, 4.47. Found: C, 53.82; H, 4.27. Calcd for Os(PhCH$_2$x)$_2$(PPh$_3$)$_2$, $OsC_{52}H_{44}O_2S_4P_2$: C, 57.77; H, 4.07. Found: C, 57.51; H, 4.01.

***trans*-Bis(methylxanthato)bis(triphenylphosphine)osmium(III) Hexafluorophosphate Dihydrate, *trans*-[Os(Mex)$_2$(PPh$_3$)$_2$]PF$_6$·2H$_2$O.** To a solution of 100 mg (0.11 mmol) of pure *cis*-Os(Mex)$_2$(PPh$_3$)$_2$ in 30 mL of dichloromethane–acetonitrile (1:10) was added 95 mg (0.15 mmol) of ceric ammonium sulfate dissolved in 20 mL of water. The mixture was stirred at room temperature for 1 h. The color of the solution became bluish green. The reaction mixture was then filtered and the filtrate reduced to 10 mL under reduced pressure. A saturated aqueous solution of NH_4PF_6 (10 mL) was added. The deep green solid thus obtained was collected by filtration, washed with water, and dried in vacuo over P_4O_{10}. The crude product was dissolved in a minimum volume of dichloromethane and was subjected to chromatography on a silica gel (60–120 mesh, BDH) column (20 × 1 cm). On elution with benzene–acetonitrile (9:1) a deep bluish green band moved out very fast and was collected. The required complex was obtained from the eluent in crystalline form by slow evaporation.

Anal. Calcd for [Os(Mex)$_2$(PPh$_3$)$_2$]PF$_6$·2H$_2$O, $OsC_{40}H_{40}O_4S_4P_3F_6$: C, 43.27; H, 3.61. Found: C, 43.50; H, 3.52. Calcd for [Os(Etx)$_2$(PPh$_3$)$_2$]PF$_6$·2H$_2$O, $OsC_{42}H_{44}O_4S_4P_3F_6$: C, 44.32; H, 3.87. Found: C, 44.11; H, 3.92. Calcd for [Os(*i*-Prx)$_2$(PPh$_3$)$_2$]PF$_6$·2H$_2$O, $OsC_{44}H_{48}O_4S_4P_3F_6$: C, 45.31; H, 4.12. Found: C, 45.41; H, 4.06. Calcd for [Os(PhCH$_2$x)$_2$(PPh$_3$)$_2$]PF$_6$·2H$_2$O, $OsC_{52}H_{48}O_4S_4P_3F_6$: C, 49.48; H, 3.81. Found: C, 49.30; H, 3.72.

***trans*-Bis(methylxanthato)bis(triphenylphosphine)osmium(II), *trans*-Os(Mex)$_2$(PPh$_3$)$_2$.** A 100-mg (0.11-mmol) amount of *trans*-[Os(Mex)$_2$(PPh$_3$)$_2$]PF$_6$·2H$_2$O was dissolved in acetonitrile (20 mL) and stirred magnetically at 273 K under a stream of nitrogen. Hydrazine hydrate (35 mg, 0.7 mmol) is 5 mL of acetonitrile was added dropwise. The bluish green solution immediately changed to red, and a solid separated out. The stirring was continued for 15 min. The red solid thus obtained was collected by filtration. The mass was washed with water and acetonitrile and dried in vacuo over P_4O_{10}, affording *trans*-Os(Mex)$_2$(PPh$_3$)$_2$.

Anal. Found for Os(Mex)$_2$(PPh$_3$)$_2$: C, 51.62; H, 3.70. Found for Os(Etx)$_2$(PPh$_3$)$_2$: C, 52.87; H, 4.07. Found for Os(*i*-Prx)$_2$(PPh$_3$)$_2$: C, 53.41; H, 4.30. Found for Os(PhCH$_2$x)$_2$(PPh$_3$)$_2$: C, 57.60; H, 4.21.

Treatment of EPR Data. The details of the method used for assigning the observed EPR signals can be found in our recent publications.[8] We note that a second solution also exists that is different from the chosen one, having small distortions and ν_1 and ν_2 values. The near-IR results clearly eliminate this solution as unacceptable.

Kinetic Measurements. Isomerization of **2** → **1** was monitored spectrophotometrically in thermostated cells. For the determination of k^{II}, increase in absorption (A_t) at 360 nm was digitally recorded as a function of time (t). A_∞ was measured when intensity changes leveled off. Values of first-order rate constants, k^{II}, were obtained from the slopes of linear least-squares plots of $-\ln (A_\infty - A_t)$ against t. A minimum of 30 $A_t - t$ data points were used for each calculation. The isomerization of $\mathbf{1}^+ \rightarrow \mathbf{2}^+$ was followed electrochemically. The cathodic current height due to the couple $\mathbf{1}^+/\mathbf{1}$ was monitored as a function of switching potential, and the rate constants, k^{III}, were computed according to the available procedure.[11] The activation parameters, ΔH^* and ΔS^*, were obtained from the Eyring plot.[21]

X-ray Structure Determination. Single crystals were grown (298 K for **1a** and $\mathbf{2a}^+$ and 273 K for **2a**) as follows: *cis*-Os(Mex)$_2$(PPh$_3$)$_2$ (**1a**), slow diffusion of dichloromethane solution into hexane followed by slow

Table VII. Crystallographic Data for *cis*-Os^{II}(Mex)$_2$(PPh$_3$)$_2$ (**1a**), *trans*-Os^{II}(Mex)$_2$(PPh$_3$)$_2$ (**2a**), and *trans*-[Os^{III}(Mex)$_2$(PPh$_3$)$_2$]PF$_6$·2H$_2$O ($\mathbf{2a}^+$)

	1a	**2a**	$\mathbf{2a}^+$
chem formula	$C_{40}H_{36}O_2P_2S_4Os$	$C_{40}H_{36}O_2P_2S_4Os$	$C_{40}H_{40}O_4F_6P_3S_4Os$
fw	929.1	929.1	1110.1
space group	*Pbca*	$P\bar{1}$	$P\bar{1}$
a, Å	10.774 (3)	9.231 (4)	9.766 (4)
b, Å	18.580 (7)	10.466 (5)	11.363 (5)
c, Å	38.043 (6)	11.149 (5)	11.677 (5)
α, deg	90	101.33 (3)	112.19 (4)
β, deg	90	108.66 (3)	105.13 (4)
ν, deg	90	108.02 (3)	97.17 (4)
V, Å^3	7616 (4)	916.8 (7)	1121.6 (9)
Z	8	1	1
T, °C	22 ± 1	20 ● 1	21 ± 1
λ	0.71073	0.71073	0.71073
ρ_{calcd}, g cm^{-3}	1.621	1.683	1.643
μ, cm^{-1}	36.80	38.21	31.92
transm coeff	0.211–0.288	0.748–1.000	0.702–0.864
R^a	0.0457	0.0544	0.0475
$R_w{}^b$	0.0530	0.0744	0.0578

$^a R = \sum||F_o| - |F_c||/\sum|F_o|$. $^b R_w = [\sum w(|F_o| - |F_c|)^2/\sum w|F_o|^2]^{1/2}$; $w^{-1} = \sigma^2(|F_o|) + g|F_o|^2$; g = 0.0007 for **1a**, 0.0035 for **2a**, and 0.0005 for $\mathbf{2a}^+$.

(16) (a) Harman, W. D.; Fairlie, D. P.; Taube, H. *J. Am. Chem. Soc.* **1986**, *108*, 8223–8227. (b) Harman, W. D.; Sekine, M.; Taube, H. *J. Am. Chem. Soc.* **1988**, *110*, 2439–2445.
(17) Dwyer, F. P.; Hogarth, J. W. *Inorg. Synth.* **1957**, *5*, 204–209.
(18) Hoffman, P. R.; Caulton, K. G. *J. Am. Chem. Soc.* **1975**, *97*, 4221–4228.
(19) Vogel, A. I. *A Text Book of Practical Organic Chemistry*, 3rd ed.; ELBS and Longman Group Ltd: London, 1965.
(20) (a) Chakravarty, A. R.; Chakravorty, A. *J. Chem. Soc., Dalton Trans.* **1982**, 615–622. (b) Mahapatra, A. K.; Datta, S.; Goswami, S.; Mukherjee, M.; Mukherjee, A. K.; Chakravorty, A. *Inorg. Chem.* **1986**, *25*, 1715–1721.
(21) Wilkins, R. G. *The Study of Kinetics and Mechanism of Reactions of Transition Metal Complexes*; Allyn and Bacon, Inc.: Boston, MA, 1974.

Table VIII. Atomic Coordinates (×10⁴) and Equivalent Isotropic Displacement Coefficients (Å² × 10³) (with Their Estimated Standard Deviations in Parentheses) for *cis*-$Os^{II}(Mex)_2(PPh_3)_2$[a]

atom	x	y	z	U(eq)
Os	129 (1)	2756 (1)	3711 (1)	35 (1)
P(1)	1596 (4)	2950 (2)	3270 (1)	35 (2)
P(2)	1398 (4)	2620 (3)	4193 (1)	38 (2)
S(3)	−170 (4)	4019 (2)	3797 (1)	41 (1)
S(2)	−1523 (4)	2606 (3)	3272 (1)	55 (2)
S(4)	−1599 (4)	2939 (3)	4120 (1)	52 (2)
S(1)	−376 (4)	1504 (3)	3662 (1)	54 (2)
O(1)	−2329 (13)	1195 (9)	3292 (3)	83 (4)
O(2)	−2189 (11)	4287 (7)	4181 (3)	62 (4)
C(1)	−1489 (17)	1745 (11)	3390 (5)	54 (5)
C(2)	−3368 (20)	1442 (13)	3094 (5)	101 (8)
C(3)	−1376 (16)	3805 (10)	4057 (4)	53 (5)
C(4)	−1977 (18)	5049 (10)	4129 (5)	77 (6)
C(6)	1 (16)	3905 (9)	2911 (4)	51 (4)
C(8)	137 (17)	4234 (9)	2301 (4)	56 (5)
C(32)	313 (17)	1021 (10)	5082 (5)	63 (6)
C(34)	−199 (16)	1600 (9)	4537 (4)	53 (5)
C(36)	2300 (15)	4007 (10)	4336 (4)	51 (5)
C(35)	1566 (14)	3442 (8)	4458 (4)	39 (4)
C(39)	936 (16)	4187 (11)	4945 (5)	70 (6)
C(40)	895 (15)	3519 (10)	4763 (4)	49 (5)
C(5)	998 (14)	3441 (9)	2878 (4)	38 (4)
C(10)	1541 (17)	3391 (9)	2554 (5)	55 (5)
C(7)	−478 (17)	4285 (9)	2620 (4)	56 (5)
C(30)	1745 (17)	1838 (10)	4816 (4)	58 (5)
C(31)	1425 (18)	1360 (10)	5080 (5)	66 (6)
C(33)	−482 (17)	1121 (10)	4811 (5)	65 (6)
C(9)	1085 (17)	3794 (11)	2267 (5)	64 (6)
C(29)	937 (14)	1951 (9)	4535 (4)	41 (4)
C(37)	2351 (16)	4650 (10)	4514 (5)	58 (5)
C(38)	1643 (17)	4742 (11)	4816 (5)	63 (6)
C(19)	3526 (15)	4790 (10)	3533 (4)	46 (5)
C(21)	4893 (16)	3833 (9)	3650 (3)	48 (4)
C(17)	2874 (15)	3577 (9)	3404 (4)	43 (4)
C(25)	5183 (16)	2220 (10)	4256 (4)	60 (5)
C(22)	3989 (13)	3343 (9)	3528 (4)	36 (4)
C(11)	2456 (12)	2226 (10)	3048 (4)	35 (4)
C(26)	5298 (17)	1664 (10)	4023 (4)	65 (5)
C(18)	2633 (14)	4305 (9)	3402 (4)	38 (4)
C(16)	3579 (16)	2326 (12)	2874 (4)	59 (5)
C(20)	4613 (16)	4536 (10)	3658 (4)	61 (5)
C(23)	2988 (14)	2249 (10)	4133 (4)	47 (4)
C(13)	2446 (18)	990 (12)	2822 (5)	70 (6)
C(24)	4027 (14)	2544 (9)	4309 (4)	43 (4)
C(12)	1860 (17)	1566 (10)	3014 (4)	54 (5)
C(28)	3144 (15)	1685 (9)	3907 (4)	50 (5)
C(15)	4107 (19)	1781 (11)	2681 (5)	67 (6)
C(27)	4352 (17)	1419 (10)	3862 (5)	59 (5)
C(14)	3557 (19)	1133 (12)	2666 (5)	75 (7)

[a] Equivalent isotropic U defined as one-third of the trace of the orthogonalized U_{ij} tensor.

evaporation; *trans*-$Os(Mex)_2(PPh_3)_2$ (**2a**) and *trans*-$[Os(Mex)_2(PPh_3)_2]PF_6 \cdot 2H_2O$ (**2a**$^+$), same as **1a** but without the evaporation step. Data collection was performed on a Nicolet R3m/V automated diffractometer using graphite-monochromated MoKα radiation (λ = 0.71073 Å). Significant crystal data and data collection parameters are listed in Table VII. The unit cell parameters were determined by least-squares fit of up to 25 reflections selected from rotation photographs. Lattice dimensions and the Laue groups were checked by axial photography. Systematic absences led to the identification of the space group as *Pbca* for **1a**. Both **2a** and **2a**$^+$ structures were solved in the space group $P\bar{1}$. In each case two check reflections were measured after every 98 reflections during data collection to monitor the crystal stability. No significant intensity reduction was observed in the 104 and 76 h of exposure to X-rays for **1a** and **2a**, respectively. But in the case of **2a**$^+$ intensities decreased by 30% in the 99 h of exposure. All data were corrected for decay (decay correction ranges on intensities were as follows: **1a**, 0.9770–1.0164; **2a**, 0.8880-1.0100; **2a**$^+$, 0.6293–1.0000) and Lorentz–polarization effects. An empirical absorption correction was done on **1a** and **2a** on the basis of azimuthal scans.[22]

(22) North, A. C. T.; Philips, D. C.; Mathews, F. S. *Acta Crystallogr. Sect. A* **1968**, *A24*, 351–359.

Table IX. Atomic Coordinates (×10⁴) and Equivalent Isotropic Displacement Coefficients (Å² × 10³) (with Their Estimated Standard Deviations in Parentheses) for *trans*-$Os^{II}(Mex)_2(PPh_3)_2$[a]

atom	x	y	z	U(eq)
Os	0	0	0	22 (1)
P(1)	−2006 (3)	73 (2)	−1909 (2)	27 (1)
S(2)	−776 (3)	1374 (2)	1491 (2)	31 (1)
S(1)	1422 (3)	2489 (2)	358 (2)	32 (1)
O(1)	669 (9)	4180 (7)	1877 (7)	45 (3)
C(15)	−3142 (10)	1174 (9)	−1555 (8)	29 (3)
C(9)	−1234 (11)	850 (10)	−3043 (9)	33 (4)
C(3)	−3714 (11)	−1652 (10)	−3058 (9)	34 (4)
C(1)	444 (11)	2852 (9)	1334 (8)	31 (3)
C(16)	−2481 (13)	2621 (11)	−1359 (10)	40 (4)
C(20)	−4603 (11)	628 (11)	−1340 (10)	39 (4)
C(4)	−4640 (12)	−2516 (10)	−2543 (11)	42 (4)
C(10)	406 (12)	1176 (11)	−2870 (9)	37 (4)
C(17)	−3238 (14)	3465 (11)	−984 (11)	47 (5)
C(14)	−2265 (14)	1120 (12)	−4099 (10)	44 (5)
C(8)	−4089 (14)	−2131 (12)	−4441 (10)	48 (5)
C(13)	−1688 (17)	1685 (13)	−4951 (11)	56 (6)
C(19)	−5328 (12)	1484 (12)	−967 (11)	45 (4)
C(11)	990 (14)	1768 (12)	−3723 (11)	49 (5)
C(12)	−46 (17)	1997 (13)	−4786 (11)	54 (6)
C(2)	−450 (15)	4393 (12)	2497 (12)	56 (5)
C(6)	−6292 (15)	−4246 (13)	−4747 (15)	65 (6)
C(7)	−5379 (17)	−3405 (13)	−5259 (13)	63 (6)
C(18)	−4672 (14)	2920 (12)	−793 (12)	52 (5)
C(5)	−5927 (13)	−3806 (11)	−3408 (14)	57 (6)

[a] Equivalent isotropic U defined as one-third of the trace of the orthogonalized U_{ij} tensor.

Table X. Atomic Coordinates (×10⁴) and Equivalent Isotropic Displacement Coefficients (Å² × 10³) (with Their Estimated Standard Deviations in Parentheses) for *trans*-$[Os^{III}(Mex)_2(PPh_3)_2]PF_6 \cdot 2H_2O$[a]

atom	x	y	z	U(eq)
Os	0	0	0	29 (1)
P(1)	439 (2)	2174 (2)	30 (2)	31 (1)
S(2)	−2360 (3)	−1 (2)	201 (2)	41 (1)
S(1)	321 (3)	1077 (2)	2272 (2)	42 (1)
P(2)	5000	0	5000	83 (2)
O(1)	−2146 (8)	1274 (7)	2738 (7)	61 (4)
C(9)	702 (10)	2176 (7)	−1467 (8)	33 (4)
C(3)	−1060 (9)	2929 (8)	273 (8)	34 (4)
C(1)	−1509 (11)	835 (8)	1830 (9)	42 (4)
C(15)	2085 (9)	3379 (8)	1325 (8)	34 (4)
C(4)	−2477 (10)	2297 (9)	−631 (9)	43 (4)
C(10)	2085 (10)	2242 (9)	−1562 (9)	45 (4)
C(16)	2398 (11)	4639 (9)	1417 (9)	47 (4)
C(8)	−897 (11)	4029 (9)	1426 (9)	51 (5)
C(14)	−476 (11)	1953 (10)	−2574 (9)	51 (5)
C(11)	2293 (12)	2049 (11)	−2737 (11)	61 (6)
C(17)	3612 (13)	5579 (10)	2393 (10)	61 (5)
C(19)	4304 (11)	4008 (11)	3163 (9)	55 (5)
C(12)	1141 (13)	1837 (10)	−3822 (9)	58 (5)
C(5)	−3667 (11)	2799 (11)	−400 (11)	54 (5)
C(20)	3056 (10)	3064 (9)	2195 (8)	43 (4)
C(6)	−3477 (13)	3883 (12)	710 (12)	60 (6)
C(18)	4575 (12)	5252 (10)	3256 (10)	60 (5)
C(2)	−3707 (13)	1138 (13)	2312 (13)	82 (8)
C(13)	−213 (13)	1781 (12)	−3735 (10)	65 (6)
C(7)	−2114 (15)	4495 (11)	1623 (11)	66 (6)
O(1W)	8540 (7)	4849 (9)	5126 (6)	84 (5)
F(3)	5207 (15)	789 (13)	6462 (9)	190 (8)
F(2)	6220 (13)	1101 (17)	5124 (12)	226 (10)
F(1)	3871 (16)	591 (19)	4374 (23)	276 (17)

[a] Equivalent isotropic U defined as one-third of the trace of the orthogonalized U_{ij} tensor.

All calculations for data reduction, structure solution, and refinement were done on a MicroVAX II computer with the programs of SHELXTL-PLUS.[23] All structures were solved by direct methods. The

(23) Sheldrick, G. M. *SHELXTL-Plus 88, Structure Determination Software Programs*; Nicolet Instrument Corp.: 5225-2 Verona Road, Madison, WI 53711, 1988.

models were refined by full-matrix least-squares procedures. All nonhydrogen atoms were made anisotropic for **2a** and **2a**$^+$; in the case of **1a** this was done only for the atoms within the coordination sphere. Hydrogen atoms were included at their idealized positions and were refined isotropically with fixed thermal parameters. The final convergent refinement gave residuals as summarized in Table VII. The highest difference Fourier peaks were 0.56, 1.64, and 1.17 e Å^{-3} near the metal atom for **1a**, **2a**, and **2a**$^+$, respectively. Atomic coordinates and isotropic thermal parameters for the three structures are collected in Tables VIII-X.

Acknowledgment. We are grateful to the Department of Science and Technology, New Delhi, for establishing a National Single Crystal Diffractometer Facility at the Department of Inorganic Chemistry, Indian Association for the Cultivation of Science. Financial support received from the Council of Scientific and Industrial Research is also acknowledged.

Supplementary Material Available: Listings of anisotropic thermal parameters (Tables XI, XVI, and XXI), complete bond distances (Tables XII, XVII, and XXII) and angles (Tables XIII, XVIII, and XXIII), hydrogen atom positional parameters (Tables XIV, XIX, and XXIV), and structure determination summaries (Tables XV, XX, and XXV) for *cis*-$Os(Mex)_2(PPh_3)_2$, *trans*-$Os(Mex)_2(PPh_3)_2$, and *trans*-$[Os(Mex)_2(PPh_3)_2]PF_6 \cdot 2H_2O$, respectively (18 pages); listings of observed and calculated structure factors for the above three complexes (59 pages). Ordering information is given on any current masthead page.

Contribution from the Solar Energy Research Institute, Golden, Colorado 80401, and Department of Chemistry and Biochemistry, University of Colorado, Boulder, Colorado 80309

Relationship between the Bite Size of Diphosphine Ligands and Tetrahedral Distortions of "Square-Planar" Nickel(II) Complexes: Stabilization of Nickel(I) and Palladium(I) Complexes Using Diphosphine Ligands with Large Bites

Alex Miedaner,[†] R. Curtis Haltiwanger,[‡] and Daniel L. DuBois*[,†]

Received April 6, 1990

Nickel and palladium complexes of the type $[M(L_2)_2](BF_4)_2$ and $[M(L_2)(L_2')](BF_4)_2$ (where L_2 and L_2' are diphosphine ligands) have been synthesized. The lowest energy electronic absorption band for the nickel complexes decreases in energy as the bite size of the diphosphine ligand increases. Similarly, the half-wave potentials for the Ni(II/I) and Pd(II/0) couples become more positive as the bite size increases. Structural studies of $[Ni(dppm)_2](BF_4)_2$ (where dppm is bis(diphenylphosphino)methane) and $[Ni(dppb)_2](PF_6)_2$ (where dppb is 1,2-bis(diphenylphosphino)benzene) show that increasing the bite size of the diphosphine ligands results in larger tetrahedral distortions. $[Ni(dppm)_2](BF_4)_2$ ($C_{50}H_{44}B_2F_8NiP_4$) crystallizes in the monoclinic space group $P2_1/n$ with a = 11.158 (10) Å, b = 17.43 (2) Å, c = 12.849 (11) Å, β = 111.38 (7)°, V = 3228 Å^3, and Z = 2. The structure was refined to R = 0.155 and R_w = 0.201 for 1005 independent reflections with $F_o > 6\sigma(F_o)$. $[Ni(dppb)_2](PF_6)_2$ ($C_{74}H_{64}F_{12}NiP_6$) crystallizes in space group $P\bar{1}$ with a = 11.359 (6) Å, b = 13.960 (5) Å, c = 21.297 (7) Å, α = 84.69 (3)°, β = 84.79 (4)°, γ = 78.96 (3)°, V = 3298 (2) Å^3, and Z = 2. The structure was refined to R = 0.072 and R_w = 0.085 for 2333 independent reflections with $F_o > 6\sigma(F_o)$. The tetrahedral distortion observed for $[Ni(dppb)_2](PF_6)_2$ was modeled by using extended Hückel calculations. These calculations indicate that the observed distortion may have an electronic as well as a steric component. The calculations also allow rationalization of the electronic absorption spectra, electrochemical data, and the stability of the Ni(I) and Pd(I) complexes $[Ni(dppp)_2](BF_4)$ (where dppp is 1,3-bis(diphenylphosphino)propane) and $[Pd(dppx)_2](BF_4)$ (where dppx is α,α'-bis(diphenylphosphino)-*o*-xylene). Complexes containing the ligand dppm have a marked tendency to become five-coordinate, as indicated by the structural determination of $[Ni(dppm)_2(CH_3CN)](PF_6)_2$. The latter complex ($C_{59}H_{55}F_{12}NNiP_6$) crystallizes in space group $P4/m$ with a = 19.363 (4) Å, c = 15.526 (4) Å, V = 5822 (2) Å^3, and Z = 4. The structure was refined to R = 0.048 and R_w = 0.062 for 3470 independent reflections with $F_o > 6\sigma(F_o)$.

Introduction

Nickel and palladium complexes catalyze the electrochemical reduction of CO_2,[1,2] the reductive coupling of aryl halides to biphenyls and binaphthyls,[3] and the reduction of alkyl halides.[4] These reactions are thought to involve Ni(I) or Pd(I) complexes as intermediates.[1-5] Dimerization of ethylene to butene appears to involve Pd(I) intermediates,[6] and a number of stoichiometric reactions involve Ni(I), Pd(I), or Pt(I) intermediates.[7,8] Although several mononuclear Ni(I) and Pd(I) complexes are known,[9,10] our understanding of the factors important in stabilizing these complexes to disproportionation is limited.

Electrochemical studies of nickel complexes containing monodentate phosphine ligands have shown that bond formation and cleavage reactions frequently precede or follow electron transfer.[11] These reactions complicate the assessment of the relative thermodynamic stabilities of different oxidation states. Their occurrence is the result of nickel preferring different coordination numbers and different types of ligands as the oxidation state changes. The coordination number of Ni(0) and Ni(I) phosphine complexes is normally 4, and the I/0 redox couple is reversible in most cases.[11] Nickel(II) complexes frequently have coordination

[†]Solar Energy Research Institute.
[‡]University of Colorado.

(1) Beley, M.; Collin, J. P.; Romain, R.; Sauvage, J. P. *J. Am. Chem. Soc.* **1986**, *108*, 7461.
(2) DuBois, D. L.; Miedaner, A. *J. Am. Chem. Soc.* **1987**, *109*, 113. DuBois, D. L.; Miedaner, A. Unpublished results.
(3) Semmelhack, M. F.; Helquist, P. M.; Jones, L. D.; Keller, L.; Mendelson, L.; Ryono, L. S.; Smith, J. G.; Stauffer, R. D. *J. Am. Chem. Soc.* **1981**, *103*, 6460. Semmelhack, M. F.; Helquist, P. M.; Jones, L. D. *J. Am. Chem. Soc.* **1971**, *93*, 5908. Troupel, M.; Rollin, Y.; Sibille, S.; Fauvarque, J. F.; Perichon, J. *J. Chem. Res., Synop.* **1980**, 26. Schiavon, G.; Bontempelli, G.; Corain, B. *J. Chem. Soc., Dalton Trans.* **1981**, 1074. Saraev, V. V.; Schmidt, F. K.; Larin, G. M.; Thach, V. S.; Lipovich, V. G. *Bull. Acad. Sci. USSR, Div. Chem. Sci.* (*Engl. Transl.*) **1974**, *23*, 2549.
(4) Stolzenberg, A. M.; Stershic, M. T. *J. Am. Chem. Soc.* **1988**, *110*, 5397.
(5) Amatore, C.; Jutand, A. *Organometallics* **1988**, *7*, 2203. Colon, I.; Kelsey, D. R. *J. Org. Chem.* **1986**, *51*, 2627. Tsou, T. T.; Kochi, J. K. *J. Am. Chem. Soc.* **1979**, *101*, 6319; **1979**, *101*, 7547.
(6) Ghosh, A. K.; Kevan, L. *J. Am. Chem. Soc.* **1988**, *110*, 8044.
(7) Kamer, A. V.; Osborn, J. A. *J. Am. Chem. Soc.* **1974**, *96*, 7832. Stille, J. K.; Lau, K. *Acc. Chem. Res.* **1977**, *10*, 434. Lappert, M. F.; Lendor, P. W. *Adv. Organomet. Chem.* **1976**, *14*, 345.
(8) Ram, M. S.; Bakac, A.; Espenson, J. H. *Inorg. Chem.* **1988**, *27*, 4231; **1988**, *27*, 2011. Bernhardt, P. V.; Lawrence, G. A.; Sauster, D. F. *Inorg. Chem.* **1988**, *27*, 4055.

0020-1669/91/1330-0417$02.50/0